

# WO<sub>3</sub> nanospheres with improved catalytic activity for visible light induced cross dehydrogenative coupling reactions

Shujing Li<sup>a,b,\*</sup>, Deepak Prakash Shelar<sup>c,1</sup>, Chun-Chao Hou<sup>c</sup>, Qian-Qian Chen<sup>c</sup>, Pan Deng<sup>b</sup>, Yong Chen<sup>c,\*\*</sup>

<sup>a</sup> Beijing Advanced Innovation Center for Food Nutrition and Human Health, Beijing Technology and Business University, Beijing 100048, PR China

<sup>b</sup> Department of Chemistry, School of Science, Beijing Technology and Business University, Beijing 100048, PR China

<sup>c</sup> Key Laboratory of Photochemical Conversion and Optoelectronic Materials, Technical Institute of Physics and Chemistry & University of Chinese Academy of Sciences, Chinese Academy of Sciences, Beijing 100190, PR China



## ARTICLE INFO

### Keywords:

Tungsten oxide  
Heterogeneous catalysis  
Photoredox  
C–C Coupling reaction

## ABSTRACT

Three tungsten oxides (WO<sub>3</sub>-W1 to WO<sub>3</sub>-W3) with different morphologies were prepared and characterized by XRD, SEM, TEM and HR-TEM measurements. The as-synthesized tungsten oxides were screened as photocatalysts for visible-light-driven cross dehydrogenative coupling (CDC) reactions along with commercially available WO<sub>3</sub>-W4. Preliminary studies showed that WO<sub>3</sub>-W1 with hollow sphere morphology efficiently photocatalyzed oxidative C–H functionalization as compared to other tested samples, by using molecular oxygen as a benign oxidant. The superior photocatalytic performance of WO<sub>3</sub>-W1 can be attributed to its larger surface area and pore structure which was supported by nitrogen adsorption-desorption measurements. Further, this protocol was used to synthesize  $\alpha$ -functionalized tertiary amines in good to excellent yields by irradiating a mixture of WO<sub>3</sub>-W1, tertiary amine, and nucleophiles (nitromethane or ketones) to visible light under aerobic conditions. Moreover, WO<sub>3</sub>-W1 can be recycled and reused with no obvious change in catalytic activity, indicating that this is an environmentally friendly and economical protocol and also underlines the robustness of the catalysts in light mediated cross dehydrogenative coupling reactions. It is hoped that our results could offer useful information for designing of new heterogeneous semiconductors for photoredox catalytic organic reactions.

## 1. Introduction

Visible-light photoredox catalysis has attracted much attention in organic synthetic community because it is environmentally benign and has promising industrial applications [1–8]. In this context, asymmetric alkylation of aldehydes [9–11], [2 + 2] cycloaddition of enones [12–14], [3 + 2] cycloaddition of aryl cyclopropyl ketones [15–17], reductive dehalogenation [18,19], radical addition to unsaturated bonds [20–22], and coupling reactions [23–26] have been successfully achieved. Among all these reactions, C–C bond forming reaction is the most extensively studied reaction. Especially, CDC reaction has attracted considerable interest among the C–C bond forming reactions because it does not require substrate prefunctionalization and is thus atom economic [27–30]. Recently, photo-induced C–C bond forming reactions have been conducted by using molecular ruthenium or iridium complexes as photocatalysts [29–31]. However, practical applications of these photocatalysts are hampered because of their high costs

and the difficulty in separating them from reaction mixtures. Furthermore, ruthenium and iridium compounds are highly toxic and suspected carcinogens and these metals are scarce. For these reasons, the identification of more convenient visible-light photocatalysts has become an area of intense research. As a result of these efforts, several reports have appeared where the commonly used Ru(II) and Ir(III) polypyridyl complexes as catalysts are avoided. In this regard, organic dyes [32–34] as well as heterogeneous semiconductors [35] have been applied to the C–C bond forming reactions to avoid the use of expensive metals and the presence of traces of metals in final products.

Photocatalysts based on heterogeneous semiconductors [36–39] have found some applications in the catalysis of organic reactions [35,40–44]. Moreover, heterogeneous photocatalyst have ability to recover and reuse and thus eliminate the contamination of the organic product. For example, carbon nitride has been explored as an intriguing catalyst for photoredox reactions due to its polymeric feature and facile synthesis. Zhang et al., have summarized the application of carbon

\* Corresponding author at: Beijing Advanced Innovation Center for Food Nutrition and Human Health, Beijing Technology and Business University, Beijing 100048, PR China.

\*\* Corresponding author.

E-mail addresses: [lishujing@mail.ipc.ac.cn](mailto:lishujing@mail.ipc.ac.cn) (S. Li), [chenyong@mail.ipc.ac.cn](mailto:chenyong@mail.ipc.ac.cn) (Y. Chen).

<sup>1</sup> These authors contributed equally to this work.

nitride in this field [45]. In addition, titanium dioxide is by far the most-attractive photocatalytic materials owing to its low cost, excellent chemical and photochemical stability, low toxicity, and high reactivity [46,47]. However, because of its wide band gap ( $> 3$  eV),  $\text{TiO}_2$  responds only to UV light, which seriously limits its use in visible-light-driven photocatalysis. Although several C–C, C–H, or C–heteroatom bond forming reactions [48–50] and even asymmetric  $\alpha$ -alkylation reactions of aldehydes that are promoted by visible light in the presence of  $\text{TiO}_2$  have been reported, these reactions proceeded with low efficiency [35]. In turn, low-band-gap semiconductors such as  $\text{PbBiO}_2\text{Br}$  [35] have been used as efficient visible-light photocatalysts for the C–C coupling reactions. However, the toxicity of this material severely limits its practical use. Inspired by these results, we have endeavored to identify inexpensive, recyclable, environmentally benign, abundant heterogeneous catalyst with narrow band gap.

Tungsten oxide ( $\text{WO}_3$ ) is one of the important members of transition metal oxides and has attracted considerable attention because it possesses wide range of applications in electrochromic windows [51], optical devices [51], electrochromic (EC) devices [52], photocatalysis [53], and gas sensing [54]. With a suitable band gap (2.7 eV),  $\text{WO}_3$  is also an important visible-light-responsive photocatalyst and has been widely used in the photocatalytic degradation of organic pollutants [55,56]. Recently, efforts have been made to synthesize nanostructured  $\text{WO}_3$  for application in supercapacitors (SCs) and lithium-ion battery (LIBs) [57,58]. Undertaking these reports and our continuous interest in identification of less expensive photocatalyst [59], we herein report that  $\text{WO}_3$  can be useful in visible light mediated cross dehydrogenative coupling reactions as a robust and efficient photocatalyst. The as-synthesized nanosphere  $\text{WO}_3$ -W1 with a surface area of  $14.1 \text{ m}^2/\text{g}$  and main porous radius size distribution of 25.8 nm exhibited enhanced activity in CDC reaction. Moreover,  $\text{WO}_3$  has been successfully reused for at least five consecutive cycles without any loss of catalytic activity and composition which revealed the robustness of the catalysts in light mediated cross dehydrogenative coupling reactions.

## 2. Materials and methods

### 2.1. Materials

Commercially available reagents and solvents were used without further purification unless indicated otherwise. The solvents used for photophysical measurements were of HPLC grade. All the *N*-aryltetrahydroisoquinolines **1** needed for CDC reactions were prepared by using the reported procedure [60] and purified through column chromatography. The commercial  $\text{WO}_3$  (bulk material) was purchased from Aladdin Industrial Corporation.

### 2.2. Synthesis of materials

#### 2.2.1. Synthesis of tungsten oxides ( $\text{WO}_3$ ) with different morphologies

The nanosphere  $\text{WO}_3$  was synthesized using a pyrolysis of  $\text{W}_{18}\text{O}_{49}$  precursor method [61]. In a typical procedure, a  $\text{W}^{6+}$  precursor ( $\text{WCl}_6$ , 2 g) was dissolved in 100 mL absolute ethanol, and the transparent solution was then transferred to the Teflon-lined stainless steel autoclave and heated at  $180^\circ\text{C}$  for 24 h. The obtained blue precipitate was collected by centrifugation and washed several times by ethanol, followed by drying under vacuum for 12 h. Then, this dry precipitate was further annealed in air at  $550^\circ\text{C}$  in a box furnace for 2 h, after which the nanosphere  $\text{WO}_3$  was obtained. The same procedure was used to prepare sea-urchin like nano  $\text{WO}_3$  except the concentration of  $\text{WCl}_6$  precursor is  $0.5 \text{ g}/100 \text{ mL}$ .

The hollow-shell vesicle  $\text{WO}_3$  was synthesized using the PVA@Glau hybrid polymer as template. The PVA@Glau was synthesized as followed: PVA (1 g, polyvinyl alcohol, DP =  $1750 \pm 50$ ) and glucose (3 g) were dissolved in 100 mL distilled water under a heated temperature until a clear solution was obtained. Then the transparent

solution was transferred to a Teflon-lined autoclave, which was then sealed and maintained at  $180^\circ\text{C}$  for 24 h. After cooling to room temperature, the obtained black product was collected by centrifugation and rinsed several times by water and ethanol. Then the as-prepared PVA@Glau (1 g) and  $\text{WCl}_6$  (0.8 g) were soaked in anhydrous ethanol (30 mL) and sealed, stirred in an ice-water bath for 12 h, followed by filtration. After dried in vacuum, the obtained sample was heated from room temperature to  $450^\circ\text{C}$  over 7 h and annealed at  $450^\circ\text{C}$  for a further 1 h in air to obtain the final yellow product.

#### 2.2.2. General procedure for the CDC reaction of nitroalkanes with tetrahydroisoquinolines

A mixture of 2-phenyl-1,2,3,4-tetrahydroisoquinoline (42 mg, 0.2 mmol), and  $\text{WO}_3$ -W1 (10 mg) was dissolved in nitromethane (10 mL) in a 15 mL Pyrex tube equipped with a rubber septum and magnetic stir bar. The mixture was bubbled with a stream of oxygen for 30 min. The tube was then sealed and irradiated by a 0.5 W LED lamp at ambient temperature. The progress of the reaction was monitored by thin-layer chromatography at regular intervals. After 24 h of irradiation, solvent was removed under vacuum, and the residue was purified by column chromatography on silica gel to afford the corresponding products.

#### 2.2.3. General procedure for the Mannich reaction of acetone with tetrahydroisoquinolines

A mixture of 2-phenyl-1,2,3,4-tetrahydroisoquinoline (42 mg, 0.2 mmol),  $\text{WO}_3$ -W1 (10 mg) and *L*-proline (4.6 mg, 0.04 mmol) was dissolved by a mixture of acetone (6 mL) and  $\text{CH}_3\text{OH}$  (4 mL) in a 15 mL Pyrex tube equipped with a rubber septum and magnetic stir bar. The mixture was bubbled with a stream of oxygen for 30 min. The tube was then sealed and irradiated by a 0.5 W LED lamp at ambient temperature. After 24 h of irradiation, solvent was removed under vacuum, and the residue was purified by column chromatography on silica gel to afford the corresponding products.

### 2.3. Characterization

Electrospray Ionization (ESI) mass spectra were performed on a Finnigan LCQ quadrupole ion trap mass spectrometer (samples were dissolved in HPLC grade methanol).  $^1\text{H}$ ,  $^{13}\text{C}$  and  $^{19}\text{F}$  NMR spectra were recorded using a Bruker Avance DP X 400 MHz instrument. LED light:  $\lambda > 420 \text{ nm}$ , 0.5 W x 30. The emission spectrum of the LED light is as shown in Fig. S1.

#### 2.3.1. TEM, HR-TEM, SEM and SEM-EDX measurements

The powder samples were dispersed in ethanol solutions which were sonicated for at least 30 min. Subsequently the suspended sample was dropped and placed on an ultra-thin carbon film copper mesh and allowed to dry in the air at room temperature. The TEM, HRTEM measurements were performed on a TEM (JEM 2100F) which was operated at an accelerating voltage of 200 kV. The scanning electron microscopes (SEM) and Energy-dispersion X-ray spectroscopy (EDX) measurements were performed on the HITACHI S-4800.

#### 2.3.2. X-ray diffraction

Powder X-ray diffraction (PXRD) analysis was carried out on a diffractometer (Bruker D8 Focus) using  $\text{CuK}\alpha$  radiation ( $\lambda = 1.5406 \text{ \AA}$ ) between  $5^\circ$  and  $90^\circ$  ( $2\theta$ ).

#### 2.3.3. $\text{N}_2$ -physisorption

The  $\text{WO}_3$  samples were dried at  $150^\circ\text{C}$  on a vacuum line for more than 24 h before the measurement. BET surface areas were measured by  $\text{N}_2$  adsorption and desorption at 77 K on a Quadrasorb SI-MP Analyzer from Quantachrome Instrument Company and analyzed by means of a computer using quadrasorb win software. The pore size distribution was calculated by the BJH method and all the total pore volumes of  $\text{WO}_3$  were calculated at 0.9 relative pressures.

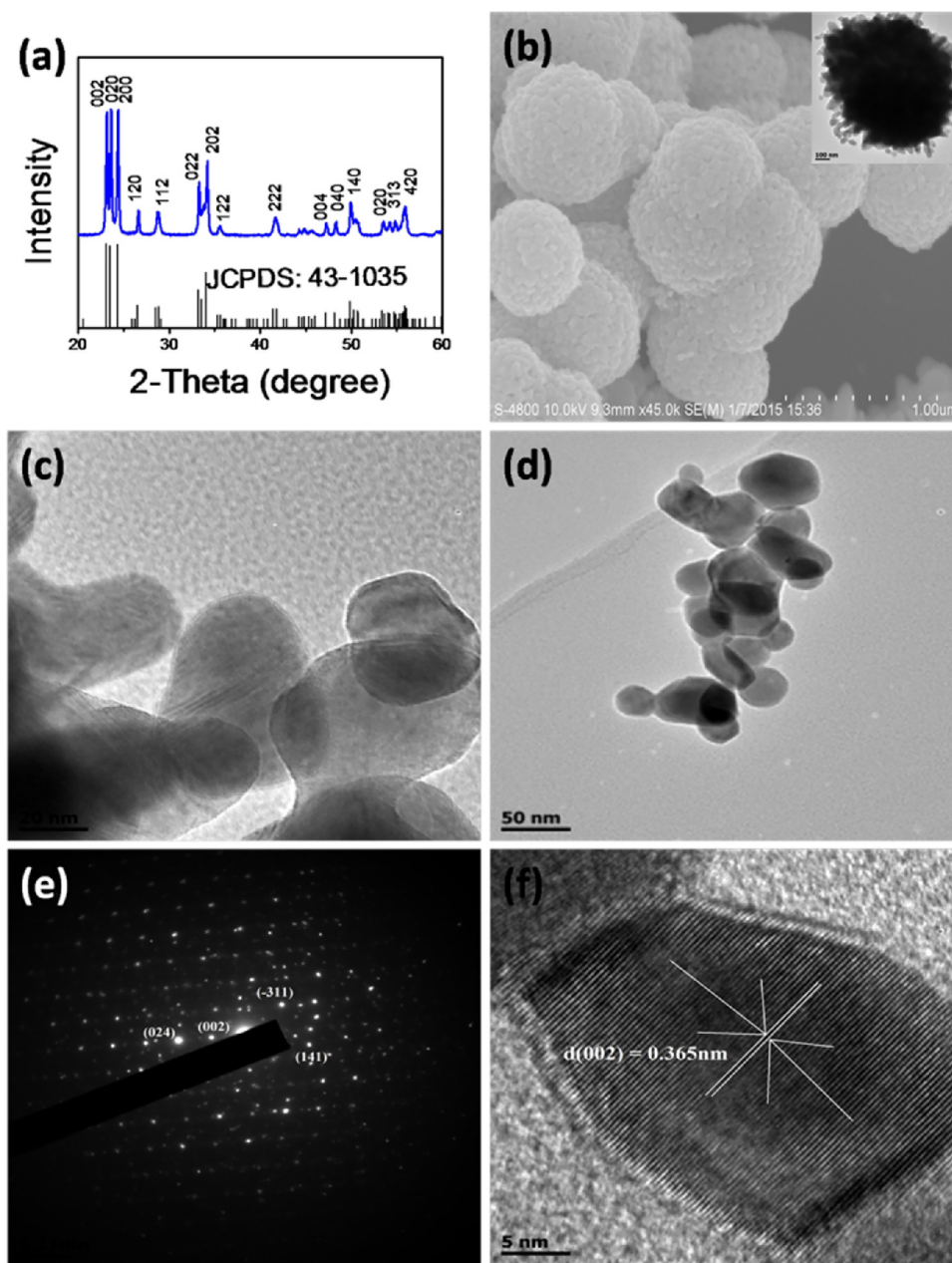


**Fig. 1.** Characterizations of nanosphere  $\text{WO}_3\text{-W1}$ . (a) Powder XRD pattern. (b) SEM image, Inset: the corresponding TEM image. (c) Magnified TEM image of the surface of nanosphere. (d) TEM for the nanoparticles of  $\text{WO}_3$ . (e) SAED pattern and (f) HRTEM image.

#### 2.3.4. ESR measurement

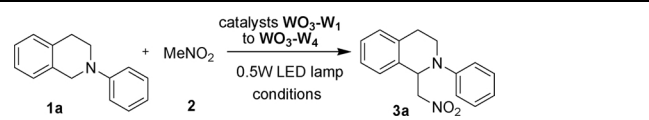
ESR spectra were recorded at room temperature using a Bruker ESP-300E spectrometer at 9.8 GHz, X-band with 100 Hz field modulation. Samples were quantitatively injected into specially made quartz capillaries for ESR analysis before being purged with argon or oxygen for 30 min in the dark and illuminated directly in the cavity of the ESR spectrometer with a 100 W mercury lamp.

### 3. Results and discussion

Three nanoscale tungsten oxide materials ( $\text{WO}_3\text{-W1}$  to  $\text{WO}_3\text{-W3}$ ) were prepared according to literature methods (see experimental section). The as-synthesized samples were first confirmed by the X-ray diffraction (XRD) analysis (Fig. 1a and S2). The entire diffraction peaks agree well with the reported JCPDS (43-1035) card, which can be indexed to the pure monoclinic phase of  $\text{WO}_3$ . No other impurities were detected in the prepared products. The UV-vis spectrum shows the

adsorption edge at 470 nm, demonstrating that the obtained  $\text{WO}_3$  nanoparticles have sufficient adsorption under visible light irradiation (Fig. S3). Scanning electron microscopy (SEM) and transmission electron microscope (TEM) analyses were performed to examine the morphology of the as-prepared  $\text{WO}_3$  samples and commercial  $\text{WO}_3\text{-W4}$ . SEM and TEM images clearly showed that the  $\text{WO}_3\text{-W1}$  has a sphere-like structure with a diameter of 500 nm (Fig. 1b). A close inspection revealed that these sphere-like structures are composed of nanoparticles with a size of 20–30 nm (Figs. 1c, d, S3). From the HR-TEM, it is clear that the  $\text{WO}_3\text{-W1}$  has lattice spacing of about 0.365 nm, which corresponds to the monoclinic  $\text{WO}_3$  phase (002) face (Fig. 1f). Selected area electron diffraction (SAED) pattern of  $\text{WO}_3$  nanoparticles showed sharp and ordered spots, which can be indexed to (002), (-311), (024) and (141) planes of monoclinic  $\text{WO}_3$  (Fig. 1e). Moreover, the energy disperse X-ray analysis (EDX) in random areas of  $\text{WO}_3\text{-W1}$  demonstrated that W and O elements were abundantly present in the nanosphere sample (Fig. S5). Other  $\text{WO}_3$  with different morphologies were also

**Table 1**  
Optimization of CDC reaction of tetrahydroisoquinoline **1a** with nitromethane.



| Entry          | Conditions <sup>a</sup>       | Conv. [%] <sup>b</sup> | Yield [%] <sup>c</sup> |
|----------------|-------------------------------|------------------------|------------------------|
| 1              | WO <sub>3</sub> -W1           | 100                    | 96                     |
| 2              | WO <sub>3</sub> -W2           | 100                    | 88                     |
| 3              | WO <sub>3</sub> -W3           | 100                    | 82                     |
| 4              | WO <sub>3</sub> -W4           | 59                     | 44                     |
| 5              | WO <sub>3</sub> -W1 in air    | 100                    | 76                     |
| 6              | No light, WO <sub>3</sub> -W1 | 0                      | 0                      |
| 7 <sup>e</sup> | WO <sub>3</sub> -W1           | trace                  | trace                  |
| 8              | No catalyst                   | 15                     | 12                     |

<sup>d</sup>Isolated yield based on **1a**.

<sup>a</sup> Reaction conditions: **1a** (0.2 mmol), CH<sub>3</sub>NO<sub>2</sub> (10 mL) and 10 mg of photocatalyst. The reaction was saturated with O<sub>2</sub> before irradiation unless indicated otherwise; reaction time of 24 h.

<sup>b</sup> After reaction, the solvent was evaporated, and the residue was subjected to <sup>1</sup>H NMR spectroscopic analysis. Conversions were determined by crude <sup>1</sup>H NMR spectroscopic analysis using 4,4'-dimethyl-2,2'-bipyridine as an internal standard and are based on **1a**.

<sup>c</sup> Yields on the basis of the starting amount of **1a** and were determined by <sup>1</sup>H NMR analysis.

<sup>e</sup> The reaction was deoxygenated.

characterized and confirmed (Figs. S5, S7 and S8). On the basis of all characterization including XRD, SEM, TEM and HRTEM, we assigned the synthesized WO<sub>3</sub> along with commercially available WO<sub>3</sub> as WO<sub>3</sub>-W1: nanospheres, WO<sub>3</sub>-W2: sea-urchin like, WO<sub>3</sub>-W3: hollow-shell vesicle and commercially available WO<sub>3</sub>-W4: bulk materials.

Although the application of tungsten oxides in photocatalytic degradation of organic pollutants is well-known [54,55], their use as a catalyst for organic synthesis has been neglected. Therefore, the as-synthesized WO<sub>3</sub> along with commercially available WO<sub>3</sub> were screened for their use in light-mediated organic reactions as photocatalyst. Initially, the aza-Henry reaction was selected as a test reaction to apply WO<sub>3</sub> as inorganic heterogeneous photocatalyst. The time course of photocatalytic CDC reaction over WO<sub>3</sub>-W1 was given in Fig. S9. Quite gratifyingly, full conversion was achieved in 24 h for all tested WO<sub>3</sub> but WO<sub>3</sub>-W1 with hollow sphere morphology showed slightly better catalytic performance than others (Table 1, entries 1–3). We next explored the use of commercial WO<sub>3</sub>-W4 powder in the reaction. Under previously tested reaction conditions only 59% conversion was recorded after 24 h and the desired aza-Henry product **3a** was obtained with a low yield of 44% (Table 1, entry 4). When oxygen was replaced by air, the system also worked well but slightly lower yield was obtained (Table 1, entry 5). Control experiments showed that the reaction

did not proceed in the dark (Table 1, entry 6) and gave trace amount of conversion and product in the absence of oxygen (Table 1, entry 7). Finally we examined the viability of the reaction in the absence of a photocatalyst. When the reaction mixture was irradiated for 24 h in the absence of a semiconductor, only 15% conversion was observed (Table 1, entry 8). These last results (Table 1, entries 6–8) clearly show that nanostructured WO<sub>3</sub> employed in this study are real photocatalyst and especially WO<sub>3</sub> with nanosphere morphology facilitates the C–C bond formation under irradiation with visible light under aerobic conditions. It should be noted that other visible light responsive semiconductors including CdS, BiVO<sub>4</sub>, BiOI were also tested for this reaction, and it was found that these semiconductors are less efficient relative to WO<sub>3</sub> under the same experimental conditions.

To understand the difference of photocatalytic performance of these tungsten oxides with various morphologies, we have tested their BET surface areas and pore structures through nitrogen adsorption-desorption measurements. In general, large specific surface areas and wide pore size distributions of photocatalysts can provide more surface active sites and make charge carrier transport easier, thus leading to an enhancement of the photocatalytic performance. Fig. 2 shows the nitrogen adsorption-desorption isotherms and the corresponding BJH pore size distribution for all samples. All these isotherms belonged to type IV hysteresis loops at relative pressure of P/P<sub>0</sub> above 0.8, indicating the formation of mesoporous structure. Based on the nitrogen adsorption-desorption isotherms in Fig. 2a, the surface area of WO<sub>3</sub>-W1, WO<sub>3</sub>-W2, WO<sub>3</sub>-W3, and WO<sub>3</sub>-W4 is determined to be ca. 14.1, 7.5, 25.4, and 3.5 m<sup>2</sup> g<sup>-1</sup>, respectively. Furthermore, Fig. 2b shows that the pore size distribution is narrow and determined to be 29.0 and 34.0 nm for WO<sub>3</sub>-W1 and WO<sub>3</sub>-W2, respectively, while WO<sub>3</sub>-W3 and WO<sub>3</sub>-W4 do not show the pore size distribution with certain order. Therefore, it seems that the observed photoactivity order, i.e., WO<sub>3</sub>-W1 > WO<sub>3</sub>-W2 > WO<sub>3</sub>-W3 > WO<sub>3</sub>-W4, could be correlated closely with the two aspects: the surface area and the pore size distribution. The highest photoactivity WO<sub>3</sub>-W1 shows a rather large surface area and wide pore size distribution.

With the optimized reaction conditions established, we then investigated the scope of this protocol (Table 2). In general, different *N*-aryltetrahydroisoquinolines **1a–h** were examined in the light-mediated WO<sub>3</sub>-W1 catalyzed oxidative aza-Henry reaction. It is found that electron-donating as well as electron-withdrawing groups on the aromatic rings are compatible under the reaction conditions. They can uniformly furnish the desired products **3a–h** in good to excellent yields (Table 2). This new protocol allows an economic and cheap oxidative cross dehydrogenative coupling reaction with respect to metal-catalyzed photochemical reaction.

According to our control experimental results (Table 1, entries 6–8) and literature reports [62], the reaction mechanism of WO<sub>3</sub> photocatalyzed aza-Henry reaction is proposed (Scheme 1). Briefly, upon visible light irradiation, photogenerated electrons in the conduction

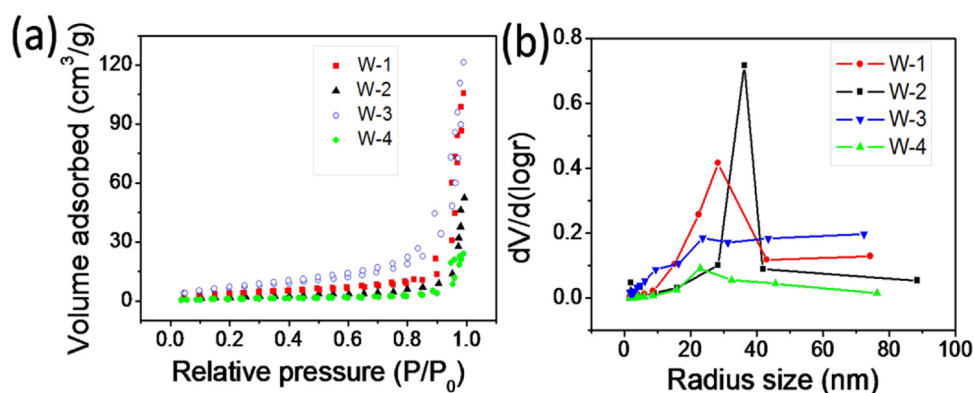
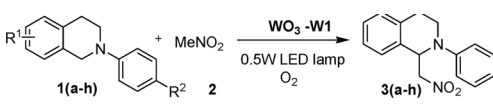


Fig. 2. (a) Nitrogen adsorption-desorption isotherm. (b) The corresponding BJH pore size distribution curve of WO<sub>3</sub>.

**Table 2**  
Substrate scope of the oxidative aza-Henry reaction.<sup>a</sup>



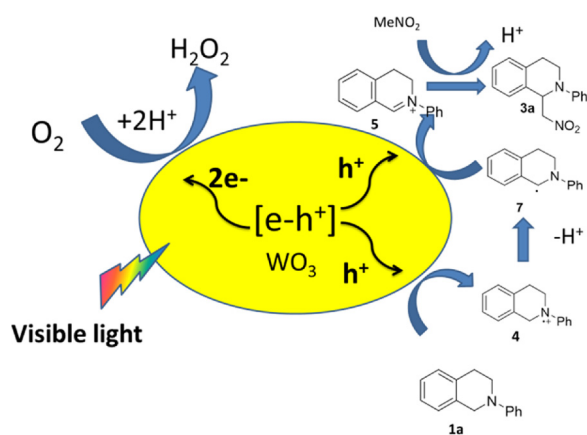
| Entry | Substrate | R <sup>1</sup>   | R <sup>2</sup>   | Conv. <sup>b</sup> | Yield <sup>c</sup>   |
|-------|-----------|------------------|------------------|--------------------|----------------------|
| 1     | 1a        | H                | H                | 100                | 96 (91) <sup>d</sup> |
| 2     | 1b        | H                | CH <sub>3</sub>  | 100                | 94 (88) <sup>d</sup> |
| 3     | 1c        | H                | OCH <sub>3</sub> | 100                | 90 (87) <sup>d</sup> |
| 4     | 1d        | H                | Cl               | 100                | 94 (88) <sup>d</sup> |
| 5     | 1e        | H                | Br               | 100                | 88 (82) <sup>d</sup> |
| 6     | 1f        | H                | F                | 100                | 90 (84) <sup>d</sup> |
| 7     | 1g        | OCH <sub>3</sub> | H                | 100                | 84 (77) <sup>d</sup> |
| 8     | 1h        | OCH <sub>3</sub> | Br               | 100                | 78 (70) <sup>d</sup> |

<sup>a</sup> Reaction conditions: **1** (0.2 mmol), **WO<sub>3</sub>-W1** (10 mg), nitroalkane (10 mL), irradiated at ambient temperature in the presence of oxygen for 24 h.

<sup>b</sup> After reaction, the solvent was evaporated, and the residue was subjected to <sup>1</sup>H NMR spectroscopic analysis. Conversions were determined by crude <sup>1</sup>H NMR spectroscopic analysis using 4,4'-dimethyl-2,2'-bipyridine as an internal standard and are based on **1**.

<sup>c</sup> Yields on the basis of the starting amount of **1** and were determined by <sup>1</sup>H NMR analysis.

<sup>d</sup> Isolated yields based on substrate **1**.



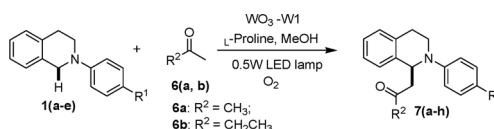
**Scheme 1.** Proposed reaction mechanism for aerobic photocatalytic aza-Henry reaction catalyzed by **WO<sub>3</sub>**.

band (CB) of **WO<sub>3</sub>** enable **O<sub>2</sub>** to undergo a two-electron transfer process ( $E_0(\text{O}_2/\text{H}_2\text{O}_2) = +0.695$  vs NHE), which is thermodynamically permissible. An ESR spin-trapping technique was employed to confirm our mechanism. After the addition of substrate **1a**, the radical signal was obviously observed (Fig. S10). Meantime, photogenerated holes in the valance band (VB) of **WO<sub>3</sub>** are reductively quenched by tertiary amine **1a** via a single electron transfer process to form an aminyl cation radical **4**. Hydrogen abstraction of aminyl cation radical **4** by radical gives the iminium ion **5**. Finally, iminium ion **5** can undergo nucleophilic addition to provide desired product **3a**.

To further evaluate the catalytic performance of **WO<sub>3</sub>-W1** and to underline the efficiency of this heterogeneous photocatalyst, we extended this protocol to the oxidative Mannich reaction. This reaction is fundamentally an important carbon-carbon bond-forming reaction in organic synthesis and offers a practical approach to valuable  $\beta$ -amino ketones. When **WO<sub>3</sub>-W1** was used to catalyze the photochemical oxidative reaction of amine (**1a-e**) with acetone in the presence of a co-catalyst, *L*-proline [23], the corresponding Mannich-type products were obtained in good to excellent yields (Table 3, entries 1–5). When acetone was replaced by methyl-ethyl ketone, similar products could be obtained in moderate to good yields (Table 3, entries 6–8)

After identifying inexpensive, readily available, heterogeneous

**Table 3**  
Mannich reaction of *N*-aryltetrahydroisoquinolines with ketone.<sup>a</sup>



| Entry | Substrate | R <sup>1</sup>  | R <sup>2</sup>                  | Conv. <sup>b</sup> | Yield <sup>c</sup>   |
|-------|-----------|-----------------|---------------------------------|--------------------|----------------------|
| 1     | 1a        | H               | CH <sub>3</sub>                 | 100                | 82 (88) <sup>d</sup> |
| 2     | 1b        | CH <sub>3</sub> | CH <sub>3</sub>                 | 100                | 82 (87) <sup>d</sup> |
| 3     | 1c        | Cl              | CH <sub>3</sub>                 | 100                | 80 (86) <sup>d</sup> |
| 4     | 1d        | Br              | CH <sub>3</sub>                 | 100                | 76                   |
| 5     | 1e        | F               | CH <sub>3</sub>                 | 100                | 79 (85) <sup>d</sup> |
| 6     | 1f        | H               | CH <sub>2</sub> CH <sub>3</sub> | 100                | 76                   |
| 7     | 1g        | CH <sub>3</sub> | CH <sub>2</sub> CH <sub>3</sub> | 100                | 70                   |
| 8     | 1h        | Cl              | CH <sub>2</sub> CH <sub>3</sub> | 100                | 72                   |

<sup>a</sup> Reaction conditions: **1** (0.2 mmol), **WO<sub>3</sub>-W1** (10 mg), *L*-proline (0.04 mmol), ketone (6 mL), CH<sub>3</sub>OH (4 mL), irradiated at ambient temperature in the presence of oxygen for 24 h.

<sup>b</sup> After reaction, the solvent was evaporated, and the residue was subjected to <sup>1</sup>H NMR spectroscopic analysis. Conversions were determined by crude <sup>1</sup>H NMR spectroscopic analysis using 4,4'-dimethyl-2,2'-bipyridine as an internal standard and are based on **1**.

<sup>c</sup> Isolated yields based on substrate **1**.

<sup>d</sup> Yields on the basis of the starting amount of **1** and were determined by <sup>1</sup>H NMR analysis.

catalyst for light mediated oxidative cross dehydrogenative coupling reactions, next we decided to examine reusability of **WO<sub>3</sub>-W1** by repeating the same reaction procedure using the recovered catalyst. The solid catalyst was recycled by centrifuging the residue mixture, washing with ethanol repeatedly and drying in vacuum at 50 °C for 2 h. As shown in Fig. 3b and Table S1, **WO<sub>3</sub>-W1** can be efficiently reused for at least 5 consecutive catalytic cycles without a distinct loss of its catalytic activity which proves catalytic efficiency of **WO<sub>3</sub>-W1** catalyst. To obtain information about the catalyst structure we compared the fresh and used **WO<sub>3</sub>-W1** in the photocatalytic reactions by SEM and XRD techniques. As displayed in Fig. 3a, XRD patterns of **WO<sub>3</sub>-W1** before and after photocatalytic reaction are rather identical. SEM analyses also showed that there is no significant change in the shape and composition of the catalyst (Fig S11). Therefore, the as-prepared **WO<sub>3</sub>-W1** semiconductor is a stable visible-light-driven photocatalyst for cross dehydrogenative coupling reactions.

#### 4. Conclusion

In summary, we synthesized **WO<sub>3</sub>** with different morphology and evaluated their photocatalytic activity for cross dehydrogenative coupling reactions. Among all tested **WO<sub>3</sub>**, **WO<sub>3</sub>-W1** exhibited the highest efficiency in catalyzing the CDC reaction, which can be attributed to its larger surface area and wide pore size distribution. The heterogeneous catalysts can catalyze aza-Henry and Mannich reactions in high yields, which are comparable to those of homogeneous reactions using transition metal complexes or organic dyes as catalysts. Furthermore, **WO<sub>3</sub>-W1** was successfully recycled and reused for five consecutive cycles without any loss of catalytic activity, which underlines the robustness of the catalysts in light mediated cross dehydrogenative coupling reactions.

#### Conflict of interest

The authors declare that they have no conflict of interest.

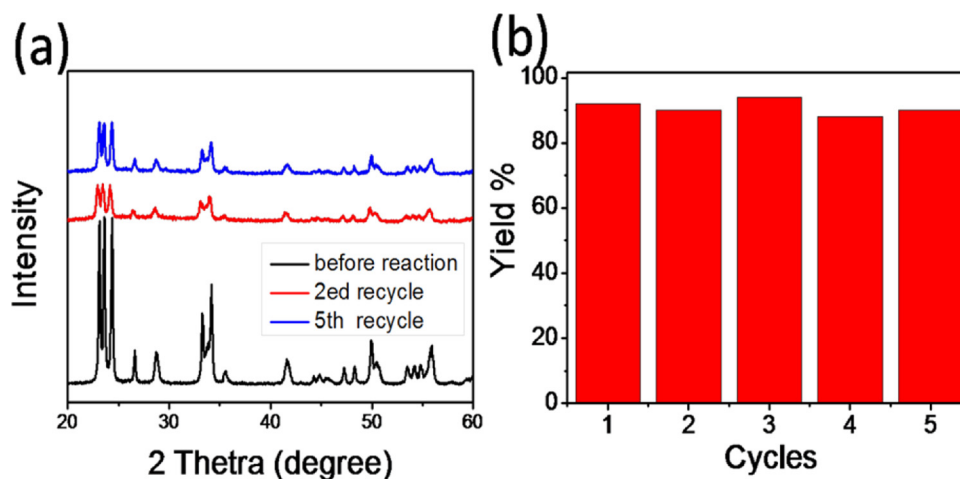


Fig. 3. (a) XRD analysis for recycled  $\text{WO}_3$ . (b) Recycling experiments for the  $\text{WO}_3$  catalyzed aza-Henry reaction between N-aryl-tetrahydroisoquinoline and nitromethane.

### Acknowledgements

This work was supported by the Strategic Priority Research Program of the Chinese Academy of Sciences (XDB17000000) and the Natural Science Foundation of China (21773275, 21371175). We thank CAS-Croucher Funding Scheme for Joint Laboratories.

### Appendix A. Supplementary data

Supplementary material related to this article can be found, in the online version, at doi: <https://doi.org/10.1016/j.jphotochem.2018.05.018>.

### References

- T.P. Yoon, M.A. Ischay, J. Du, Visible light photocatalysis as a greener approach to photochemical synthesis, *Nat. Chem.* 2 (2010) 527–532.
- J.M. Narayanan, C.R. Stephenson, Visible light photoredox catalysis: applications in organic synthesis, *Chem. Soc. Rev.* 40 (2011) 102–113.
- D. Kalyani, K.B. McMurtrey, S.R. Neufeldt, M.S. Sanford, Room-temperature C-H arylation: merger of Pd-catalyzed C-H functionalization and visible-light photocatalysis, *J. Am. Chem. Soc.* 133 (2011) 18566–18569.
- D.P. Hari, P. Schroll, B. König, Metal-free, visible-light-mediated direct C-H arylation of heteroarenes with aryl diazonium salts, *J. Am. Chem. Soc.* 134 (2012) 2958–2961.
- A. McNally, C.K. Prier, D.W. MacMillan, Discovery of an alpha-amino C-H arylation reaction using the strategy of accelerated serendipity, *Science* 334 (2011) 1114–1117.
- J.D. Nguyen, E.M. D'Amato, J.M. Narayanan, C.R. Stephenson, Engaging unactivated alkyl, alkenyl and aryl iodides in visible-light-mediated free radical reactions, *Nat. Chem.* 4 (2012) 854–859.
- X. Zhu, Z. He, Q.-Y. Li, X.-J. Wang, Direct C(sp<sup>2</sup>)-H amination of aryl aldehyde-derived hydrazones via visible light promoted photoredox catalysis, *Rsc. Adv.* 7 (2017) 25171–25174.
- P. Qian, Y. Deng, H. Mei, J. Han, J. Zhou, Y. Pan, Visible-light photoredox catalyzed oxidative/reductive cyclization reaction of N-cyanamide alkenes for the synthesis of sulfonated quinazolinones, *Org. Lett.* 19 (2017) 4798–4801.
- D.A. Nicewicz, D.W. MacMillan, Merging photoredox catalysis with organocatalysis: the direct asymmetric alkylation of aldehydes, *Science* 322 (2008) 77–80.
- M. Neumann, S. Fuldner, B. König, K. Zeitler, Metal-free, cooperative asymmetric organophotoredox catalysis with visible light, *Angew. Chem. Int. Ed.* 50 (2011) 951–954.
- P. Xu, G. Wang, Y. Zhu, W. Li, Y. Cheng, S. Li, C. Zhu, Visible-light photoredox-catalyzed C-H difluoroalkylation of hydrazones through an aminyl radical/polar mechanism, *Angew. Chem. Int. Ed.* 55 (2016) 2939–2943.
- J. Du, T.P. Yoon, Crossed intermolecular [2+2] cycloadditions of acyclic enones via visible light photocatalysis, *J. Am. Chem. Soc.* 131 (2009) 14604–14605.
- M.A. Ischay, Z. Lu, T.P. Yoon, [2+2] cycloadditions by oxidative visible light photocatalysis, *J. Am. Chem. Soc.* 132 (2010) 8572–8574.
- C. Brenninger, A. Pothig, T. Bach, Bronsted acid catalysis in visible-light-induced [2+2] photocycloaddition reactions of enone dithianes, *Angew. Chem. Int. Ed.* 56 (2017) 4337–4341.
- Z. Lu, M. Shen, T.P. Yoon, [3+2] cycloadditions of aryl cyclopropyl ketones by visible light photocatalysis, *J. Am. Chem. Soc.* 133 (2011) 1162–1164.
- L. Wang, H. Zou, X. Zhang, G. Huang, Mechanism and origins of selectivity in rhodium-catalyzed intermolecular [3+2] cycloadditions of vinylaziridines with allenes, *Organ. Chem. Front.* 4 (2017) 587–596.
- H. Huo, K. Harms, E. Meggers, Catalytic, enantioselective addition of alkyl radicals to alkenes via visible-light-activated photoredox catalysis with a chiral rhodium complex, *J. Am. Chem. Soc.* 138 (2016) 6936–6939.
- L. Furst, J.M.R. Narayanan, C.R.J. Stephenson, Total synthesis of (+)-gliocladin C enabled by visible-light photoredox catalysis, *Angew. Chem. Int. Ed.* 50 (2011) 9655–9659.
- J.D. Nguyen, J.W. Tucker, M.D. Konieczynska, C.R. Stephenson, Intermolecular atom transfer radical addition to olefins mediated by oxidative quenching of photoredox catalysts, *J. Am. Chem. Soc.* 133 (2011) 4160–4163.
- J.W. Tucker, J.M. Narayanan, S.W. Krabbe, C.R.J. Stephenson, Electron transfer photoredox catalysis: intramolecular radical addition to indoles and pyrroles, *Org. Lett.* 12 (2010) 368–371.
- A.U. Meyer, A.L. Berger, B. König, Metal-free C-H sulfonamidation of pyrroles by visible light photoredox catalysis, *Chem. Commun.* 52 (2016) 10918–10921.
- I. Ghosh, L. Marzo, A. Das, R. Shaikh, B. König, Visible light mediated photoredox catalytic arylation reactions, *Acc. Chem. Res.* 49 (2016) 1566–1577.
- M. Rueping, C. Vila, R.M. Koenigs, K. Poschary, D.C. Fabry, Dual catalysis: combining photoredox and Lewis base catalysis for direct Mannich reactions, *Chem. Commun.* 47 (2011) 2360–2362.
- P.V. Pham, D.A. Nagib, D.W. MacMillan, Photoredox catalysis: a mild, operationally simple approach to the synthesis of alpha-trifluoromethyl carbonyl compounds, *Angew. Chem.* 50 (2011) 6119–6122.
- C. Dai, J.M. Narayanan, C.R. Stephenson, Visible-light-mediated conversion of alcohols to halides, *Nat. Chem.* 3 (2011) 140–145.
- R.S. Andrews, J.J. Becker, M.R. Gagné, Investigating the rate of photoreductive glucosyl radical generation, *Org. Lett.* 13 (2011) 2406–2409.
- M. Fagnoni, D. Dondi, D. Ravelli, A. Albini, Photocatalysis for the formation of the C–C bond, *Chem. Rev.* 107 (2007) 2725–2756.
- N. Hoffmann, Photochemical reactions as key steps in organic synthesis, *Chem. Rev.* 39 (2008) 1052–1103.
- C.K. Prier, D.A. Rankin, D.W.C. MacMillan, Visible light photoredox catalysis with transition metal complexes: applications in organic synthesis, *Chem. Rev.* 113 (2013) 5322–5363.
- D.M. Schultz, T.P. Yoon, Solar synthesis: prospects in visible light photocatalysis, *Science* 343 (2014) 985–1005.
- J.A. Terrett, M.D. Clift, D.W. MacMillan, Direct beta-alkylation of aldehydes via photoredox organocatalysis, *J. Am. Chem. Soc.* 136 (2014) 6858–6861.
- Y. Pan, S. Wang, C.W. Kee, E. Dubuisson, Y. Yang, K.P. Loh, C.H. Tan, Graphene oxide and Rose Bengal: oxidative C–H functionalisation of tertiary amines using visible light, *Green Chem.* 13 (2011) 3341–3344.
- Q. Liu, Y.N. Li, H.H. Zhang, B. Chen, C.H. Tung, L.Z. Wu, Reactivity and mechanistic insight into visible-light-induced aerobic cross-dehydrogenative coupling reaction by organophotocatalysts, *Chem. Eur. J.* 18 (2012) 620–627.
- D.P. Hari, B. König, Synthetic applications of eosin Y in photoredox catalysis, *Chem. Commun.* 50 (2014) 6688–6699.
- M. Cherevatskaya, M. Neumann, S. Fuldner, C. Harlander, S. Kummel, S. Dankesreiter, A. Pfitzner, K. Zeitler, B. König, Visible-light-promoted stereoselective alkylation by combining heterogeneous photocatalysis with organocatalysis, *Angew. Chem. Int. Ed.* 51 (2012) 4062–4066.
- M.R. Hoffmann, W. Choi, D.W. Bahnemann, Environmental applications of semiconductor photocatalysis, *Chem. Rev.* 95 (1995) 69–96.
- K. Rajeshwar, N.R.D. Tacconi, C.R. Chenthamarakshan, Semiconductor-based composite materials: preparation, properties, and performance, *Chem. Mater.* 32 (2001) 2765–2782.
- N. Serpone, A.V. Emeline, Semiconductor photocatalysis - past, present, and future outlook, *J. Phys. Chem. Lett.* 3 (2012) 673–677.

- [39] H. Kisch, Semiconductor photocatalysis—mechanistic and synthetic aspects, *Angew. Chem. Int. Ed.* 52 (2013) 812–847.
- [40] N. Zeug, J. Buecheler, H. Kisch, Catalytic formation of hydrogen and C-C bonds on illuminated zinc sulfide generated from zinc dithiolenes, *J. Am. Chem. Soc.* 107 (1985) 1459–1465.
- [41] B. Ohtani, S. Kusakab, S.I. Nishimoto, M. Matsumura, Y. Nakato, Improvement of photocatalytic activity and product selectivity by cadmium metal deposited in situ on suspended cadmium(II) sulfide particles, *Chem. Lett.* 24 (1995) 803–804.
- [42] S. Marinković, N. Hoffmann, Diastereoselective radical tandem addition-cyclization reactions of aromatic tertiary amines by semiconductor-sensitized photochemical electron transfer, *Eur. J. Org. Chem.* 2004 (2004) 3102–3107.
- [43] T. Mitkina, C. Stanglmair, W. Setzer, M. Gruber, H. Kisch, B. König, Visible light mediated homo- and heterocoupling of benzyl alcohols and benzyl amines on polycrystalline cadmium sulfide, *Org. Biomol. Chem.* 10 (2012) 3556–3561.
- [44] X. Lang, X. Chen, J. Zhao, Heterogeneous visible light photocatalysis for selective organic transformations, *Chem. Soc. Rev.* 43 (2014) 473–486.
- [45] Z. Zhou, Y. Zhang, Y. Shen, S. Liu, Y. Zhang, Molecular engineering of polymeric carbon nitride: advancing applications from photocatalysis to biosensing and more, *Chem. Soc. Rev.* 47 (2018) 2298–2321.
- [46] X.B. Chen, S.S. Mao, Titanium dioxide nanomaterials: synthesis, properties, modifications, and applications, *Chem. Rev.* 38 (2007) 2891–2959.
- [47] A.L. Linsebigler, G. Lu, J.T. Yates, Photocatalysis on TiO<sub>2</sub> surfaces: principles, mechanisms, and selected results, *Chem. Rev.* 95 (1995) 735–758.
- [48] X.-H. Ho, M.-J. Kang, S.-J. Kim, E.D. Park, H.-Y. Jang, Green organophotocatalysis. TiO<sub>2</sub>-induced enantioselective  $\alpha$ -oxyamination of aldehydes, *Catal. Sci. Technol.* 1 (2011) 923–926.
- [49] M. Rueping, J. Zoller, D.C. Fabry, K. Poschary, R.M. Koenigs, T.E. Weirich, J. Mayer, Light-mediated heterogeneous cross dehydrogenative coupling reactions: metal oxides as efficient, recyclable, photoredox catalysts in C-C bond-forming reactions, *Chem. Eur. J.* 18 (2012) 3478–3481.
- [50] C. Vila, M. Rueping, Visible-light mediated heterogeneous C-H functionalization: oxidative multi-component reactions using a recyclable titanium dioxide (TiO<sub>2</sub>) catalyst, *Green Chem.* 15 (2013) 2056–2059.
- [51] J. Zhou, Y. Ding, S.Z. Deng, L. Gong, N.S. Xu, Z.L. Wang, Three-dimensional tungsten oxide nanowire networks, *Adv. Mater.* 17 (2010) 2107–2110.
- [52] Z. Xie, L. Gao, B. Liang, X. Wang, G. Chen, Z. Liu, J. Chao, D. Chen, G. Shen, Fast fabrication of a WO<sub>3</sub>·2H<sub>2</sub>O thin film with improved electrochromic properties, *J. Mater. Chem.* 22 (2012) 19904.
- [53] M. Sadakane, K. Sasaki, H. Kunioku, B. Ohtani, R. Abe, W. Ueda, Preparation of 3-D ordered macroporous tungsten oxides and nano-crystalline particulate tungsten oxides using a colloidal crystal template method, and their structural characterization and application as photocatalysts under visible light irradiation, *J. Mater. Chem.* 20 (2010) 2092–2100.
- [54] L.F. Zhu, J.C. She, J.Y. Luo, S.Z. Deng, J. Chen, N.S. Xu, Study of physical and chemical processes of H<sub>2</sub> sensing of Pt-coated WO<sub>3</sub> nanowire films, *J. Phys. Chem. C* 114 (2010) 15504–15509.
- [55] D. Chen, L. Gao, A. Yasumori, K. Kuroda, Y. Sugahara, Size- and shape-controlled conversion of tungstate-based inorganic-organic hybrid belts to WO<sub>3</sub> nanoplates with high specific surface areas, *Small* 4 (2008) 1813–1822.
- [56] G. Xi, B. Yue, J. Cao, J. Ye, Fe<sub>3</sub>O<sub>4</sub>/WO<sub>3</sub> hierarchical core-shell structure: high-performance and recyclable visible-light photocatalysis, *Chem. Eur. J.* 17 (2011) 5145–5154.
- [57] S. Yoon, E. Kang, J.K. Kim, C.W. Lee, J. Lee, Development of high-performance supercapacitor electrodes using novel ordered mesoporous tungsten oxide materials with high electrical conductivity, *Chem. Commun.* 47 (2011) 1021–1023.
- [58] S. Yoon, C. Jo, S.Y. Noh, C.W. Lee, J.H. Song, J. Lee, Development of a high-performance anode for lithium ion batteries using novel ordered mesoporous tungsten oxide materials with high electrical conductivity, *Phys. Chem. Chem. Phys.* 13 (2011) 11060–11066.
- [59] B. Wang, D.P. Shelar, X.Z. Han, T.T. Li, X. Guan, W. Lu, K. Liu, W.F. Fu, C.M. Che, Long-lived excited states of zwitterionic copper(I) complexes for photoinduced cross-dehydrogenative coupling reactions, *Chem. Eur. J.* 21 (2015) 1184–1190.
- [60] F.Y. Kwong, A. Klapars, S.L. Buchwald, Copper-catalyzed coupling of alkylamines and aryl iodides: an efficient system even in an air atmosphere, *Org. Lett.* 4 (2002) 581–584.
- [61] G. Xi, S. Ouyang, P. Li, J. Ye, Q. Ma, N. Su, H. Bai, C. Wang, Ultrathin W18O<sub>49</sub> nanowires with diameters below 1 nm: synthesis, near-infrared absorption, photoluminescence, and photochemical reduction of carbon dioxide, *Angew. Chem.* 51 (2012) 2395–2399.
- [62] B. Yuan, R. Chong, B. Zhang, J. Li, Y. Liu, C. Li, Photocatalytic aerobic oxidation of amines to imines on BiVO<sub>4</sub> under visible light irradiation, *Chem. Commun.* 50 (2014) 15593–15596.